

Quantifying Microsecond Solution-Phase Conformational Dynamics of a DNA Hairpin at the Single-Molecule Level

Alexander K. Foote,^{||} Kunihiko Ishii,^{||} Brendan Cullinane, Tahei Tahara, and Randall H. Goldsmith*



Cite This: *ACS Phys. Chem Au* 2024, 4, 408–419



Read Online

ACCESS |



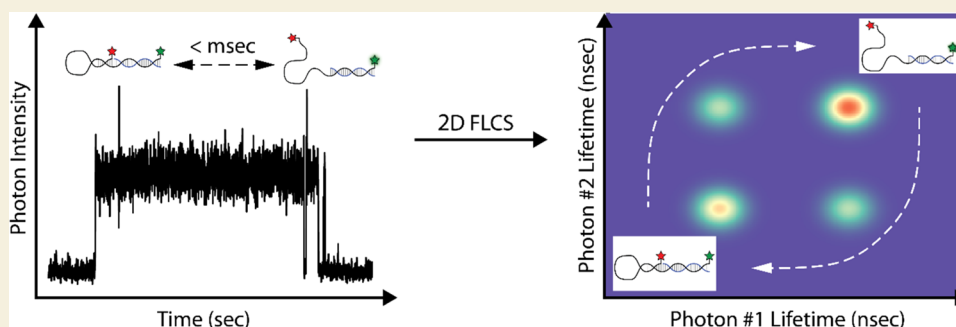
Metrics & More



Article Recommendations



Supporting Information



ABSTRACT: Quantifying the rapid conformational dynamics of biological systems is fundamental to understanding the mechanism. However, biomolecules are complex, often containing static and dynamic heterogeneity, thus motivating the use of single-molecule methods, particularly those that can operate in solution. In this study, we measure microsecond conformational dynamics of solution-phase DNA hairpins at the single-molecule level using an anti-Brownian electrokinetic (ABEL) trap. Different conformational states were distinguished by their fluorescence lifetimes, and kinetic parameters describing transitions between these states were determined using two-dimensional fluorescence lifetime correlation (2DFLCS) analysis. Rather than combining fluorescence signals from the entire data set ensemble, long observation times of individual molecules allowed ABEL-2DFLCS to be performed on each molecule independently, yielding the underlying distribution of the system's kinetic parameters. ABEL-2DFLCS on the DNA hairpins resolved an underlying heterogeneity of fluorescence lifetimes and provided signatures of two-state exponential dynamics with rapid ($<$ millisecond) transition times between states without observation of the substantially stretched exponential kinetics that had been observed in previous measurements on diffusing molecules. Numerical simulations were performed to validate the accuracy of this technique and the effects the underlying heterogeneity has on the analysis. Finally, ABEL-2DFLCS was performed on a mixture of hairpins and used to resolve their kinetic data.

KEYWORDS: conformational dynamics, single-molecule spectroscopy, Förster correlation spectroscopy, nucleic acid hairpin, fluorescence resonance energy transfer

INTRODUCTION

Complex biomolecules such as proteins or oligonucleotides constantly undergo structural changes, with local fluctuations occurring on the picosecond to nanosecond time scale, and larger conformational shifts occurring on time scales ranging from microseconds to seconds.^{1–10} Characterizing these larger structural fluctuations within a solution-phase biomolecule is an important key to understanding their function. The need is especially pressing for highly fluctuating molecules as this dynamic information is complementary to the static structural pictures offered by crystal structures and electron microscopy. If a population of biomolecules contains molecule-to-molecule heterogeneity, then elucidating fast (submillisecond) conformational fluctuations utilizing traditional bulk measurements can be very difficult.¹¹ Single-molecule Förster resonance energy transfer (SM-FRET) measurements are a powerful tool for examining the structural dynamics of

complex molecules as they bypass the limitations of ensemble-averaging in bulk measurements.^{12–15}

However, current solution-phase SM-FRET techniques have several limitations. First, use of an experimental geometry that entails freely diffusing molecules (similar to traditional fluorescence correlation spectroscopy (FCS)¹⁶) allows observation of molecules only as they rapidly diffuse through the focal volume in ~ 1 ms. This brief observation window experimentally imposes a limit on observable dynamics to those occurring faster than the occupation time scale¹² while

Received: December 4, 2023

Revised: May 3, 2024

Accepted: May 6, 2024

Published: May 29, 2024



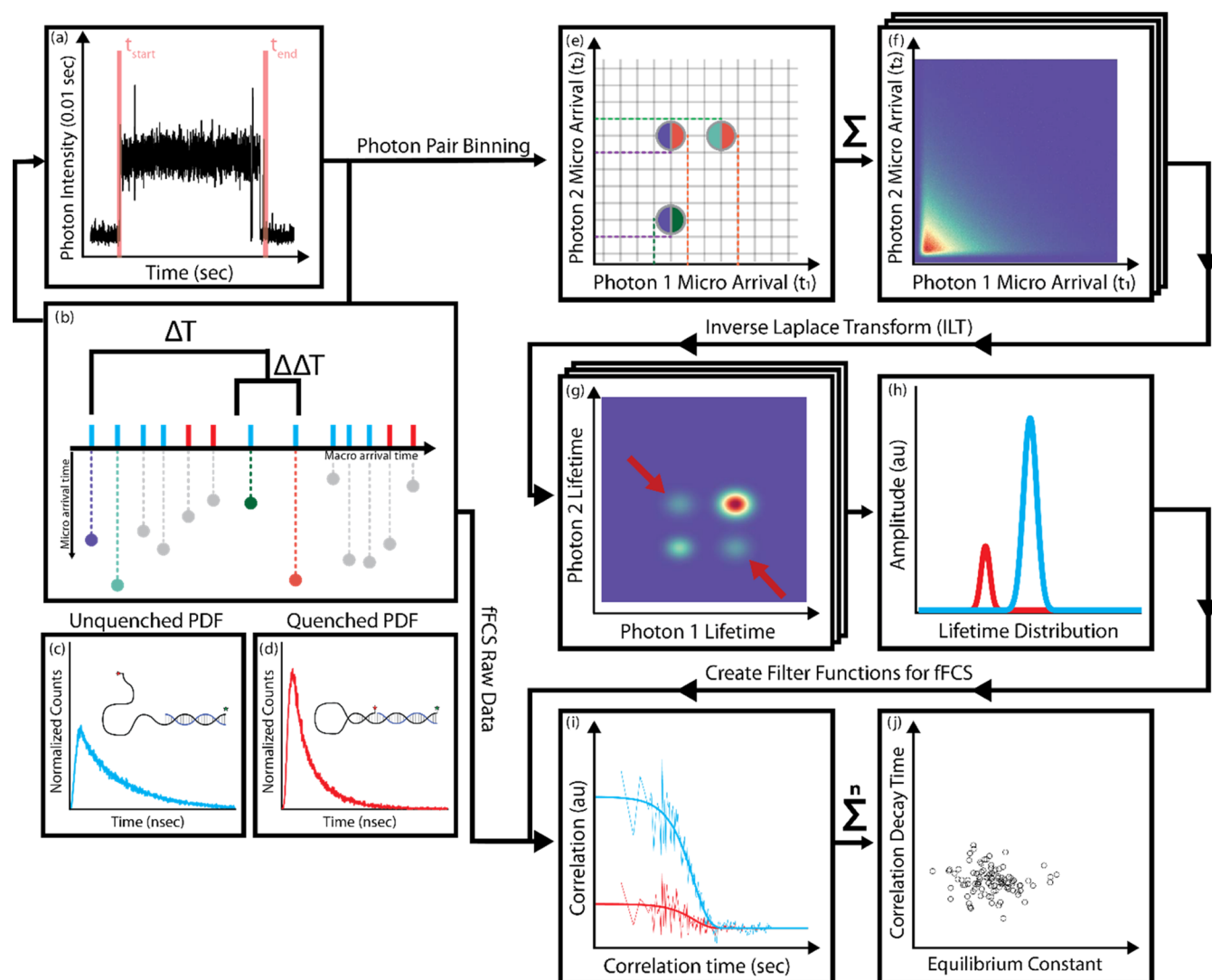


Figure 1. (a) Macrotime data is binned in intervals of 10 ms, where a change-point algorithm marks t_{start} and t_{end} of a measurement of a single molecule within the ABEL trap. (b) Representation of a photon stream. Each photon has two times corresponding to it: the macro arrival time corresponding to the time since the start of the experiment (x -axis, seconds time scale) and the micro arrival time corresponding to the most recent excitation pulse (y -axis, nanoseconds time scale). Red and blue photons represent events from the system's two different conformational states. The time window $\Delta T \pm \Delta\Delta T$ is used to determine which photons are combined to perform photon pair binning. (c, d) Representations of the micro arrival time Probability Distribution Functions for photons originating from an opened (blue) and closed (red) state. (e) An example of three photon pairs found within the $\Delta T \pm \Delta\Delta T$ window of the first two photons in panel (b). Colored dotted lines represent the micro arrival times for the corresponding photon pairs (1–7 purple–red, 1–8 purple–green, 2–8 blue–red) from panel (b) and are used to determine where the photon pairs are placed in the 2D time plot. (f) Representation of the 2D time plot after all photons within an event have been paired. An ILT is performed on the 2D time plot using maximum entropy method (MEM) to produce a 2D lifetime plot (g) and reveal the underlying distribution of lifetimes for the multiple underlying states (h). The position on the x -axis shows the lifetime distribution of each state, and the intensity along the y -axis shows its relative population. (i) Lifetime distributions from panel (h) are used as filters along with the raw photon stream from panel (b) to perform filtered fluorescence correlation spectroscopy (fFCS) measurements and produce autocorrelation decays for each population (red, blue-thin lines). Cross-correlation curves are not depicted in this example. These curves are fit with eqs 1–4 (red, blue-bold lines). (j) K_{eq} and τ_c values extracted from the fits in panel (i) for multiple single-molecule events.

also limiting the total number of photons that can be collected. Recent Bayesian-based analysis tools can help offset this limitation by reducing the number of photons required for obtaining diffusion constants¹⁷ and reaction kinetics.¹⁸ A second limitation is that conventional SM-FRET analysis methods can only access kinetic time scales slower than a millisecond, though a few techniques that rely on specific experimental conditions have achieved sub-100 μs time resolution of immobilized^{19,20} and solution-phase^{21,22} molecules. Of particular note is an innovative hidden Markov model

analysis that can measure kinetics of solution-phase molecules spanning 3 orders of magnitude.^{23–25} Importantly, all of these methods are vulnerable to a third limitation in that they require analysis over the entire ensemble of molecules to determine kinetic information, ultimately limiting their ability to determine kinetic information for molecules displaying intrinsic behavioral heterogeneity. Said another way, though raw data are acquired molecule by molecule, the dynamics extracted are from many molecules.

Among the techniques that can push the limits of accessible SM-FRET time resolution is two-dimensional fluorescence lifetime correlation spectroscopy (2DFLCS), which utilizes the lifetime information on different states to obtain key kinetic parameters.^{26,27} By using a freely diffusing FCS-like geometry and analyzing the photon-arrival time at numerous delay times, the interconversion dynamics between subpopulations of different lifetimes can be determined without prior knowledge of the system. 2DFLCS has been applied in the study of complex systems such as light-harvesting complexes,^{20,28} the B domain of protein A,²⁹ and cytochrome *c*.³⁰ The 2DFLCS methodology has been expanded to include elucidation of solvent exposure³¹ and by incorporating additional information on quenched-donor states through two-color FRET analysis.³² However, there is substantial numerical instability in this analysis when only low photon counts are available, which prevents the application of 2DFLCS to an individual diffusing molecule. Thus far, 2DFLCS has been implemented by combining data from many molecules, precluding analysis of individual molecules.

In this work, we employ an anti-Brownian electrokinetic (ABEL) trap that allows trapping and monitoring of individual fluorescent or scattering molecules in solution over the course of multiple seconds.^{33–35} Many photons are observed per molecule ($>10^5$ photons), allowing for statistically robust measurements to be performed on a molecule-by-molecule (MBM) basis. While comparable photon counts can be achieved using alternative FCS geometries by transiently binding molecules to the surface³⁶ or attaching them to slowly diffusing substrates,³⁷ these methodologies involve tethering of the biomolecule that may affect the conformational dynamics of biomolecules;^{38–41} the ABEL trap avoids possible tethering-induced artifacts by keeping the molecule in solution. Recently, the ABEL trap has been used to reveal heterogeneity in the solution-phase population of an intrinsically disordered protein through quantification of rotational dynamics,^{42,43} study FRET-based systems of DNA mixtures with shot-noise limited precision,⁴⁴ investigate photosynthetic antenna systems,^{41,45,46} characterize F1-ATP synthase enzymes⁴⁷ and the molecular motor Rep,⁴⁸ used to resolve complex mixtures based on lifetime and anisotropy,⁴⁹ expanded to allow estimation of diffusion constants,^{50,51} and trapping of nonfluorescent systems through interferometric scattering.⁵² Here, ABEL trapping is combined with subsequent 2DFLCS analysis to address the shortcomings of typical solution-phase FRET measurements by (1) extending the solution-phase observation times, (2) enabling elucidation of submillisecond dynamics, and (3) performing analysis on each individual molecule without ensemble-averaging. To test our methodology, we designed a DNA hairpin with a short (four nucleotide) stem that has opening–closing dynamics on the submillisecond time scale (Figure SI.1.1). We outline a strategy for measuring and analyzing solution-phase, single-molecule kinetics at the submillisecond time scale using 2DFLCS within an ABEL trap (ABEL-2DFLCS), and we report the first observation of submillisecond dynamics for an individual solution-phase molecule. We further demonstrate the instrumental and analytical ability to accurately obtain fast ($<ms$) kinetic parameters using simulations.

EXPERIMENTS AND METHOD

Sample Preparation and Data Acquisition

A DNA fragment containing a hairpin loop (Cy7–5′-AAGG-(T)₂₁-CCTT-GGATCCAGGACGCTA-3′-ATTO647N) (Figure SI.1.1) was labeled with a fluorophore (Atto647N) and quencher (Cy7) such that it produced two primary states with different fluorescent lifetimes of the donor: namely, an open (unquenched) and a closed (quenched) state (Figure 1c,d). The fragment contains a 21-base-pair hairpin loop, a 4-base-pair stem adjacent to the loop, and a 15-base-pair segment at the 3′ end to maintain constant distance of 15 bp between FRET dyes when in the closed conformation. A nonlabeled complement to the 15-base-pair segment was added in $\sim 10^6$ fold excess ($5 \mu M$) to maintain a constant distance from double-stranded DNA.

The mechanism of the ABEL trap has been described in detail in previous papers^{42,43} and the Supporting Information (Sections SI.1 and SI.2). Briefly, a pulsed (40 MHz, instrument response function, or IRF, shown in Section SI.2) excitation beam is rapidly scanned in a predetermined pattern through a trapping region within a microfluidic device. Each detected photon is correlated to the beam's position, allowing estimation of molecular position and application of real-time feedback voltages that induce position-compensating electrokinetic flows, canceling the Brownian motion of the molecule.

Data Analysis

The fundamental theory behind 2DFLCS has been thoroughly described^{26,27,53} and is summarized below. A graphical depiction of the 2DFLCS analysis process, from the measurement of an individual molecule's photon stream to the extraction of that molecule's kinetic parameters, is outlined in Figure 1. This figure serves as a roadmap and will be referenced throughout the paper to help establish key points in the analysis process. Fluorescence emission is detected on an avalanche photo diode detector and logged via time-correlated single-photon counting. Each detected photon has two associated arrival times: the macrotime, assigned as the time difference between the beginning of the measurement and the detection of the fluorescence photon (time scale of μs – s), and the microtime, assigned as the time difference between the most recent laser pulse and the detection of the fluorescence photon (time scale of ps–ns). The photons are assigned to 10 ms bins using their recorded macrotimes to create an intensity stream (Figure 1a, black line), and a change-point algorithm⁵⁴ is run on the binned data to determine the start and end points of the observed fluorescence signal for each molecule (Figure 1a, t_{start} and t_{end} , respectively). A graphical representation of a simulated typical photon stream created by the kinetic transition between the open and closed hairpin states is shown in Figure 1b, with the macrotimes of the open (blue) and closed (red) states shown on the *x*-axis, and their corresponding microtimes displayed on the *y*-axis. These macro and micro arrival times for all photons between each molecule's observed t_{start} and t_{end} are utilized to perform 2DFLCS analysis on each individual molecule.

A characteristic macrotime interval (corresponding to molecular dynamics in a temporal range of interest, Figure 1b, ΔT) is selected, and photon pairs whose macrotimes fall within a time window $\Delta T \pm \Delta\Delta T/2$ have their microtimes correlated with each other to create a 2D correlation plot (Figure 1b,e). The microtime of the first photon within the pair (t_1) is projected on the *x*-axis of this 2D correlation plot, and the microtime of the second photon (t_2) is projected on the *y*-axis. Three example photon pairs within the stream (Figure 1b: 1–7, 1–8, 2–8) have their microtimes' positions within the 2D correlation plot depicted in Figure 1e (purple/green, purple/orange, teal/orange). This process is repeated for every photon pair with macrotimes between t_{start} and t_{end} to create the raw 2D correlation plot (2D emission-delay correlation map, Figure 1f) after background subtraction (Section SI.3). Then, a 2D inverse Laplace transform (ILT) is performed on each correlation plot to create a 2D lifetime plot (2D lifetime correlation map) for this ΔT (Figure 1g). ILTs are known to be numerically unstable, and so this process is stabilized using a maximum entropy method (MEM) that has been extended

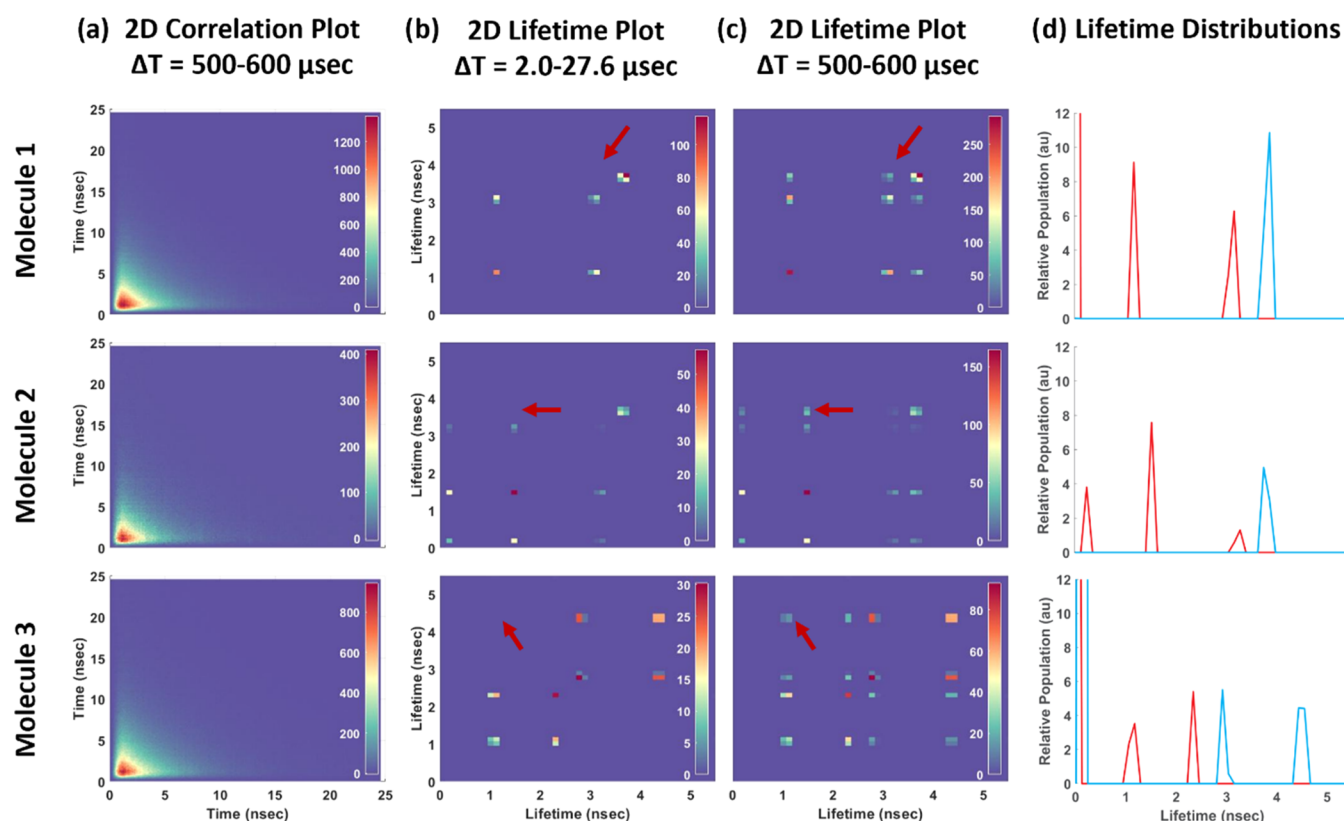


Figure 2. (a) Representative photon-arrival correlation plots for three single-molecule events. The displayed plots were created with a ΔT window of 500–600 μs , and other plots (Section SI.14) were created for shorter and longer ΔT windows. (b, c) Resulting lifetime plots from an inverse Laplace transform of the correlation plots in panel (a). The peak's x and y -locations correspond to the lifetime of the first and second photon, respectively, while the peak height corresponds to the relative number of photon pairs observed with these lifetimes (the lifetime distribution). (b) Result of a 2D correlation plot with a shorter ΔT (shown in Section SI.14), while panel (c) is the result of an inverse Laplace transforming of panel (a). (d) Lifetime distributions from the analysis of the 2D lifetime plots taken at numerous ΔT windows. These lifetime distributions are empirically derived for each individual molecule and give the filter functions for later fFCS analysis.

into 2D.^{26,55,56} Importantly, if the selected ΔT for this 2D lifetime plot is on the kinetic time scale of transition between two fluorescent states (as in the photon stream depicted in Figure 1b), the appearance of cross-peaks will be observed within the 2D lifetime plot (Figure 1g, red arrows). In practice, the MEM analysis is performed globally on 2D correlation plots created at multiple ΔT s, with the fastest kinetic window (shortest ΔT) yielding our fastest measurable independent fluorescent lifetime distribution: the lifetime distribution for each distinct fluorescent state (Figure 1h). These lifetime distributions give an empirically determined lifetime probability distribution for each observable independent fluorescent state (independent fluorescence component) within each single-molecule event, and they are free from ensemble-averaging effects imposed by heterogeneity within the system. These lifetime distributions are obtained without prior information on the system and without input from the user. The lifetime distributions of each state may be more complex than a single observed lifetime due to dye dynamics, including rapid local motion, dark states, or sticking to the construct due to hydrophobicity. Importantly, the MBM nature of this analysis process accounts for such molecular heterogeneity.

Determined fundamental lifetime distributions can then be converted into filters (Section SI.4) that compensate for background correlation and can be used in lifetime-filtered fluorescence correlation spectroscopy (fFCS).^{57,58} In fFCS, separate functions are created from the known lifetime distributions of each state, where these functions can be individually applied to the autocorrelation function in order to “filter” out the autocorrelations of each independent state. The empirically determined filters for our system can be combined with the information from the raw photon stream (on a molecule-by-molecule basis, Figure 1b) for fFCS analysis. For a

simple two-state system, this procedure results in three outputs: an autocorrelation function of each state (Figure 1i) and two identical cross-correlation functions. In the two-state system, these lifetime-filtered auto- and cross-correlation functions are governed by the kinetic interconversion of the two states and can be fit with the following equations

$$G_{1,1}(T) = G_d(T)[1 + K_{\text{eq}} \cdot G_r(T)] \quad (1)$$

$$G_{2,2}(T) = G_d(T) \left[1 + \frac{1}{K_{\text{eq}}} \cdot G_r(T) \right] \quad (2)$$

$$G_{1,2}(T) = G_d(T)[1 - G_r(T)] \quad (3)$$

$$G_r(T) = a \exp\left(-\frac{T}{\tau_r}\right) + b \quad (4)$$

Fitting yields the equilibrium constant (K_{eq}) and correlation decay time (τ_r).^{52,59} $G_d(T)$ typically accounts for the effect of diffusion, but the unique feature of the ABEL trap to enable trapping of the molecule at the center of the focal region renders this factor very close to 1, in stark contrast to previous 2DFLCS measurements that model freely diffusing molecules³² (Section SI.5). Here, the factor slightly deviates from 1 due to the slight nonuniformity of excitation at the edges of the ABEL trap excitation area. a and b in eq 4 are correction factors and are close to 1 and 0, respectively, and account for background fluorescence. This fitting process is repeated for each trapped solution-phase molecule within the data set, and the resulting K_{eq} and τ_r were scattered to visualize the distribution of parameters

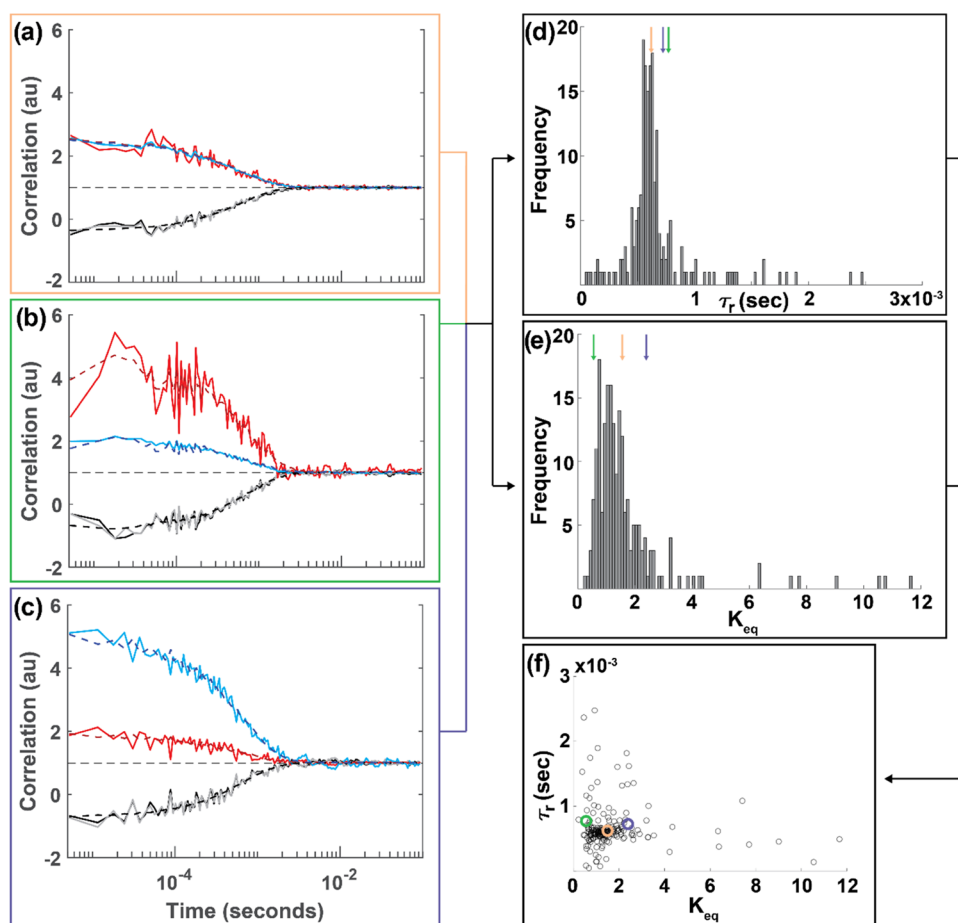


Figure 3. (a–c) Filtered autocorrelation decays for the open (blue curve) and closed (red curve) states of the three representative events. Cross-correlation curves (formed from open–closed and closed–open cross-correlation, black and gray curves, respectively) should have the same underlying shape given in eqs 1–4. Decays were made using the filters represented in Figure 2d. (d, e) Auto and cross-correlation decays were globally fit and the K_{eq} and τ_r for all events are displayed as histograms, with the relative values for the three events shown as colored arrows. (f) K_{eq} and τ_r are scattered against each other, visualizing little correlation between the two variables. The three representative events are shown by their corresponding color-highlighted points.

among the molecules (Figure 1j). Finally, the K_{eq} and τ_r can be used to easily derive the rate constants for the opening (k_{open}) and closing (k_{close}) of the system using $K_{eq} = k_{close}/k_{open}$ and $\tau_r = (k_{open} + k_{close})^{-1}$.

RESULTS AND DISCUSSION

Single-molecule solution-phase ABEL-2DFLCS measurements were performed on a DNA hairpin loop with a 4-base-pair stem and a T21 hairpin loop. Three representative molecules (total $N = 208$) were selected and their 2D correlation plots, 2D lifetime plots (for two different ΔT s), and lifetime distributions, analogous to Figure 1f–h, respectively, are shown in Figure 2. Several points demonstrating the power and utility of ABEL-2DFLCS analysis can be noted here. First, the evolution of cross-peaks at different ΔT ranges can be observed, with fewer cross-peaks occurring at fast time scales ($\Delta T = 2\text{--}27.6 \mu\text{s}$, Figure 2b, red arrows), and new, well-defined cross-peaks emerging at longer time scales ($\Delta T = 500\text{--}600 \mu\text{s}$, Figure 2c, red arrows). The cross-peaks at the smallest ΔT likely derive from rapid dye photophysics ($<1 \mu\text{s}$), while new cross-peaks at larger ΔT originate in conformational dynamics between the open and closed hairpin states. The appearance of these conformational cross-peaks clearly exhibits the ability of ABEL-2DFLCS analysis to observe interconver-

sion kinetics between distinct lifetime states at the submillisecond time scale.

A large amount of lifetime heterogeneity was observed within this seemingly simple DNA hairpin system. This diversity is most evident when observing the different x -axis values of the lifetime distributions, particularly for the quenched closed state (Figure 2d, red), as each molecule can have different lifetime distributions characterizing its fundamental fluorescence states. One possible origin of this heterogeneity between different molecules could be sticking of either the donor dye or acceptor quencher to the DNA hairpin structure. This sticking would cause variations in lifetimes between the closed states, such as the differences seen in molecules 1 and 2. The analysis below will examine whether these observed differences within the lifetime distributions are due to real experimental heterogeneity within the system or numerical instability. It should be noted that variations in the lifetime distributions may appear at very short lifetimes ($<1 \text{ ns}$) or with very small amplitudes and are likely computational artifacts due to the IRF. However, these smaller components are relatively small in magnitude and are easily filtered from further downstream (Section SI.15). The difference in the relative amplitudes of the lifetime distributions informs on the relative photon counts attributed to each underlying state.

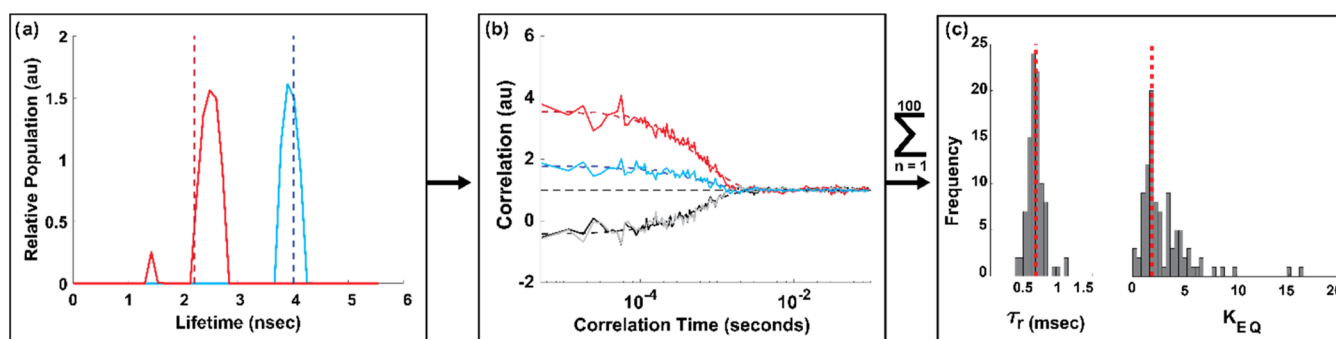


Figure 4. MBM ABEL-2DFLCS analysis performed on simulated data. (a) Lifetime distributions for the opened and closed states shown in blue and red solid lines, respectively. Known lifetime values for the states of this event are shown as dashed lines. (b) Autocorrelation decays for the opened (blue) and closed (red) states, as well as the cross-correlation decays (black and gray) shown as solid lines. Theoretical correlation decays based on the known kinetic parameters for this event are shown as dashed lines. (c) Histograms of the K_{eq} and τ_r kinetic parameters for the $N = 100$ simulated events. Known values are shown as dashed vertical red lines.

Such heterogeneity would not be observable without MBM analysis and would be lost to the ensemble during a typical FCS-type measurement. Worth noting also is the complexity of the lifetime distributions for each fluorescence state. For example, all three observed molecules have a closed state that exhibits two distinct lifetimes at the fast ($\Delta T = 2\text{--}27.6 \mu\text{s}$) time scale (Figure 2b). This profile implies that two lifetime populations exist within the closed state that rapidly equilibrate with each other on the submicrosecond time scale. Such fast fluctuations between lifetime states have been observed in multiple ensemble-based 2DFLCS experiments^{27,31} and likely derive from rapid changes in dye orientation and conformation, interactions of the dyes with the nucleotide bases,⁶⁰ or photoisomerization of the cyanine acceptor dye.⁶¹

As seen in the three representative molecules as well as consistently across the full data set, it is apparent that there are two distinct conformational states observed at the microsecond time scale: an opened and a closed state. This observation comes from the 2D lifetime plots in Figure 2 as there are only two independent states at fast ΔT that do not share cross-peaks (Figure 2b). Interconversion between these two states at longer, 100- μs time scales are clearly observed, as evidenced by the appearance of cross-peaks (Figure 2c, red arrows). Furthermore, the 2D MEM analysis requires only two independent components (Figure 2d, red and blue) to fit the 2D correlation plots and obtain lifetime distributions, suggesting there are only two observable lifetime distributions and thus two interconverting conformations.

Our observation of two independent states at fast time scales is noteworthy as numerous single-molecule FRET studies on DNA hairpin loops using traditional FCS experimental geometries have shown inconsistent results, with early efforts reporting two-state exponential dynamics,^{62,63} while a later three-state model with an unobservable, intermediate state^{37,64–68} was also proposed. Development and implementation of methods to reduce the influence of nonhomogeneous excitation due to diffusion^{64,69–71} resulted in observation of an ensemble of two-state systems exhibiting static and, potentially, dynamic heterogeneity in the fluctuation rate.^{64,70,72,73} However, in these studies, the data analysis was not molecule-by-molecule but was pooled from the photon statistics of many molecules, and the system's heterogeneity was observable as stretched exponential kinetics. However, this methodology led to several complications. First, in this limit, the precise distribution of rates cannot be uniquely extracted

from the ensemble-combined data. As will be discussed below, this distribution can be directly accessed in this current work. Second, it was later shown that, even with these procedures, diffusion through the nonhomogeneous excitation profile can result in observation of an artifactual stretched exponential,⁷⁴ making any claims about heterogeneity difficult. The nature of our ABEL trap measurement removes such artifacts. In summary, complications arising from rapid diffusion through the spatially inhomogeneous confocal volume or from heterogeneity within the DNA hairpin loop system are directly addressed by our new approach, which incorporates prolonged, MBM measurements within the ABEL trap yielding statistically robust observation of individual fluctuating DNA hairpin molecules with minimal diffusion artifacts (Section S1.5). The analysis contained within Figure 2 is substantial empirical evidence for the observation of submillisecond opening and closing hairpin dynamics and indicates that ABEL-2DFLCS analysis can identify fast dynamics within a system at the single-molecule level. Combining 2DFLCS analysis with further fFCS analysis allows the quantification of these fast kinetic parameters on a MBM basis, as shown below.

We performed fFCS analysis using filters derived from the lifetime distributions obtained through the ABEL-2DFLCS analysis of the system (Figure 3). The corresponding autocorrelation decays for the opened (blue) and closed (red) states, and the two cross-correlation decays (black, gray) for molecules 1, 2, and 3 can be seen in Figure 3a–c, respectively. The decays were fit using eqs 1–4 for each molecule separately (dashed lines), resulting in a K_{eq} and τ_r value that characterize each molecule's kinetics. These kinetic parameters were obtained for the entire data set (Figure 3d–3f) and the colors surrounding the representative molecules' correlation decays are overlaid on top of the distributions. These fFCS decays further substantiate the claim of a two-state DNA hairpin system. First, the filtered auto and cross-correlation curves follow the single-exponential decays described by the two-state system modeled by eqs 1–4, showing that our measurements are well-described by a two-state system.²⁰ Second, even without modeling the decays by fitting them, it can be seen that all of the correlation decays converge to unity at the larger (millisecond) delay times for each molecule, as expected for a two-state system. This detail suggests that each molecule reaches equilibrium rapidly on the time scale of milliseconds, and no interconversion dynamics in the ms–s are present that would be indicative of a long-lived

third state, though it should be noted that if dynamics exist, which occur much slower than our total multisecond observation time, they would remain unobserved. These two observations, as well as the absence of cross-peaks noted above in Figure 2b and the two observed lifetime distributions in the MEM analysis, formulate a strong argument for the DNA hairpin existing in two and only two independent states.

In addition to validating our observation of a two-state DNA hairpin, fFCS analysis allows us to quantify the kinetic parameters within each event by their global fits to eqs 1–4, yielding an equilibrium constant and characteristic correlation decay time for each molecule and highlighting differences between each independent measurement. There are perceived differences among the filtered autocorrelation decays of the individual molecules visible in Figure 3a–c. These differences affect the derived components (K_{eq} and τ_r) in different ways: the relative magnitude of the y -intercept values of the autocorrelation decays for the two states (K_{eq}) and the shared rate of decay of the two states (the rate of interchange between states, τ_r). The MBM differences are pronounced most clearly in the scatter plot of K_{eq} and τ_r in Figure 3f. The distribution of decay times (τ_r , Figure 3d) is seen to be quite narrow, suggesting homogeneous dynamics among the molecular population. A somewhat larger distribution of the equilibrium constants (K_{eq} , Figure 3e) is seen, corresponding to differences in the y -intercept values in the decay curves (Figure 3a–c). Instrumental noise is a significant contributor to this broad K_{eq} distribution, and is more thoroughly described below using simulation (Figure 4). Excluding outliers (<10%, Section SI.6), the kinetic parameters have values of $K_{\text{eq}} = 1.4 \pm 0.05$ and $\tau_r = 6.5 \times 10^{-4} \pm 0.2 \times 10^{-4} \text{ s}^{-1}$. These values yield an average $k_{\text{open}} = 640 \pm 30 \text{ s}^{-1}$ and $k_{\text{close}} = 900 \pm 20 \text{ s}^{-1}$, consistent with the range of bulk literature values.^{32,37} All uncertainties are stated as the standard error of the mean. We would note that observed kinetics of DNA hairpins may be affected by the dye selection,⁷⁵ making it difficult to make quantitative comparisons between systems with different labels. The entire experimental procedure outlined in this work was repeated on a second DNA hairpin system with a smaller hairpin loop (T8, Section SI.7). This alternate T8 system had a significantly higher equilibrium constant, whose precise value could not be quantitatively determined, as shown through simulation (Section SI.8). This analysis highlights an apparent limitation of this approach: in order to accurately quantify the kinetic fluctuation between individual states within a system, there must be a reasonable signal contribution from each of those states.

To properly frame the quantitative results obtained by our ABEL-2DFLCS analysis method, we repeated this analysis on a data set obtained from simulation with kinetic and lifetime parameters matching our experimental values. In other words, we performed the analysis on a data set where we knew the correct kinetic parameters and could therefore verify if the analytical methodology was accurate and numerically stable, given experimentally analogous simulated noise. Since low photon counts contribute significantly to noise due to the instability of the inverse Laplace transform, our simulated data set was created with $\sim 3\times$ fewer photons than our data set, presenting a lower limit for accuracy and precision (Section SI.9). The results of our analysis of the simulated data are shown in Figure 4 and show a high level of accuracy and precision even with the reduced photon counts. The creation of the simulated data set is comprehensively described in

Section SI.9. Briefly, a stream of photons is created of combined background and signal photons, with background intensity identical to our observed system and signal intensities governed by our measured system and relative intensities between our quenched and unquenched states. The photon stream included 100 unique events corresponding to trapped molecules, with differing lifetimes for the closed states to simulate empirically observed heterogeneity within the system. Each simulated event fluctuated between the opened (blue) and closed (red) states based on the known kinetic parameters (k_{open} , k_{close}) mentioned. The photon stream was analyzed as described above, and lifetime distributions for the two underlying states were obtained for each individual event within the simulated data trace (Figure 4a, solid red and blue), and a representative line with the known lifetime values for each event is displayed (Figure 4a, dashed red and blue). As can be seen, the lifetime distributions for the two states match the known lifetime values. The lifetime distributions were then used to create filter functions for each event, and fFCS analysis was performed giving correlation decays (Figure 4b, solid lines), with the expected correlation decays given the known kinetic parameters overlaid on top (Figure 4b, dashed). Lastly, the kinetic parameters were obtained using a global fit of eqs 1–4 for each simulated molecule, giving derived K_{eq} and τ_r values that are accurate compared to the known input values (Figure 4c). Figure 4 allows us to visualize potential errors within each step of the analysis process (Figure 4a,b) and how all combined errors (from stochastic noise, computational artifacts, IRFs, etc.) might contribute to the overall accuracy of obtaining final kinetic parameters (Figure 4c). Accounting for a few outliers (<5% of the outputs having large K_{eq} values, Figure 4c, described in detail in Section SI.6), the accuracy with which ABEL-2DFLCS obtains the known input parameters for the simulated data set grants confidence in the measured kinetic parameters for the DNA hairpin loop, and directly shows that ABEL-2DFLCS analysis can accurately extract submillisecond kinetics on a MBM basis. Lastly, as the analysis shown in Figure 4 was performed on simulations with $\sim 3\times$ fewer photons than those observed experimentally, we also performed additional analysis on simulations with equivalent/higher photon counts and found consistent improvement at these increased photon counts (Section SI.10).

The correlation functions and distributions of fluctuation times (τ_r) and equilibrium constants (K_{eq}) observed in Figure 3 can now be discussed in the context of the larger body of work on DNA hybridization dynamics. As mentioned above, no evidence is seen for three-state dynamics, with the auto- and cross-correlation traces being consistent with a two-state mechanism. Previous reports hypothesized that the typical diffusive FCS time scale was not long enough to see funneling at the millisecond time scale to a third state.^{65,68} Here, even with trapping times of multiple seconds, we see no evidence for such a state. Stretched exponential kinetics (non-Arrhenius behavior), observed by several efforts,^{64,70,72,73} can result from dynamic or static heterogeneity of fluctuation rates. In the case of dynamic heterogeneity, the heterogeneity was interpreted as originating in a shallow and dynamic potential energy landscape being rapidly navigated by the biomolecules.^{70,72,73} However, the narrow distribution in Figure 3d suggests there is negligible long-lived static heterogeneity and that the DNA molecules are able to explore a large fraction of their potential energy landscape, resulting in ergodic behavior over the trapping time scale of several seconds. Further, we see no

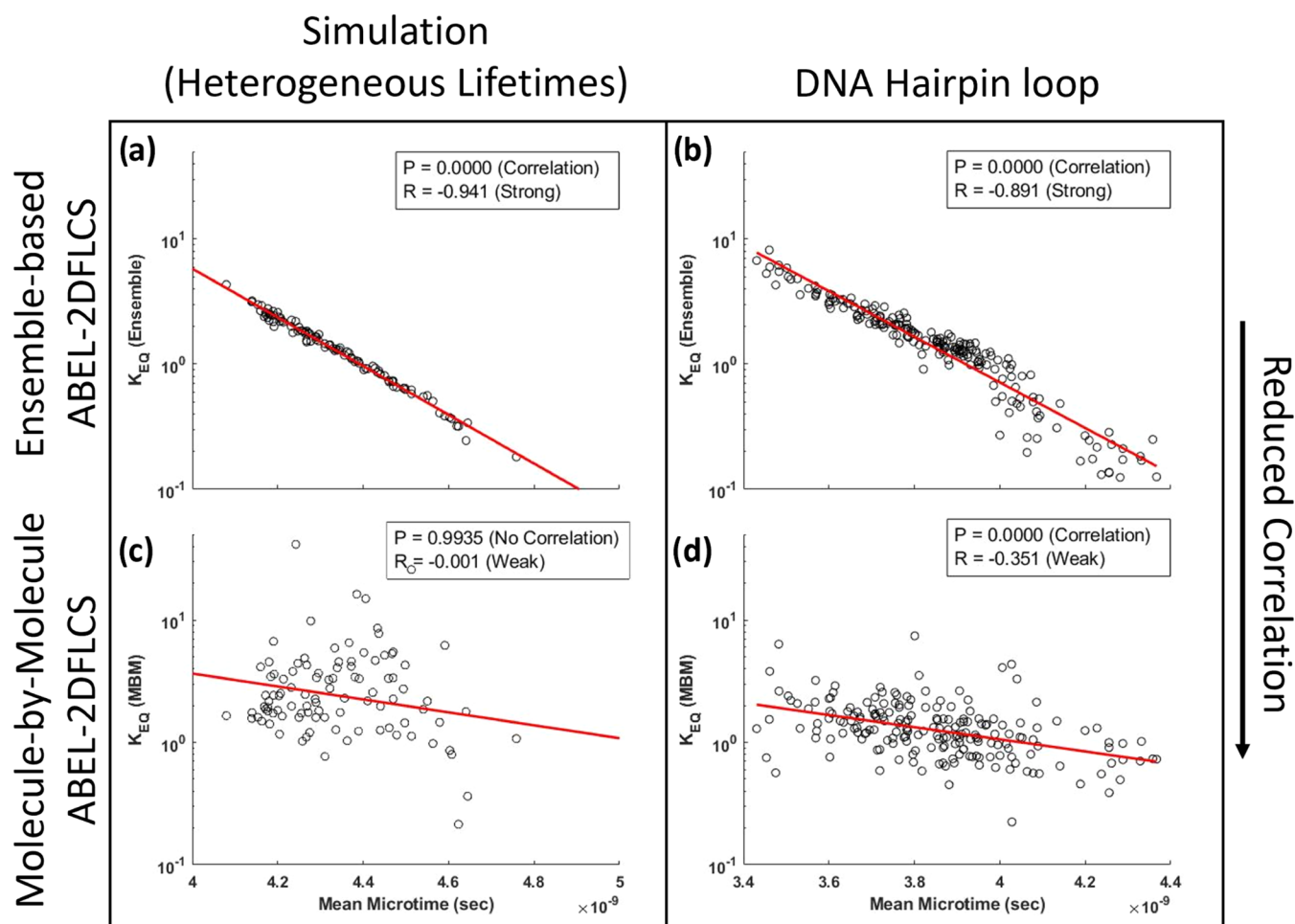


Figure 5. (a) Scatter plot of K_{eq} values derived using ensemble-based ABEL-2DFLCS against the single-exponential lifetimes for a simulated data set with heterogeneous closed-state fluorescence lifetimes. (b) Scatter plot of the ensemble-based ABEL-2DFLCS K_{eq} values against the single-exponential lifetimes for a T21 DNA hairpin. (c) Scatter plot made by performing MBM ABEL-2DFLCS analysis on the simulated data set. (d) Scatter plot made by performing MBM ABEL-2DFLCS on the T21 DNA hairpin.

evidence of dynamic heterogeneity at the level of individual molecules (Figure 3) or in ensemble-averaged data (Section SI.11): such behavior would be observable as a stretched exponential behavior in the decays, but monoexponential fits are sufficient. We note that the loop and stem sequences investigated here are in some cases similar to but not identical to those used in other studies and that dye selection can also affect the kinetics seen within DNA hairpin systems.⁷⁵ Applying ABEL-2DFLCS to a larger family of biomolecules will be the topic of future work. Finally, for biomolecules exhibiting slower interconversion dynamics and thus non-ergodic behavior,^{42,43} our approach offers a way to directly map out the static distribution in a manner that could only be obtained in MBM analyses since unique distributions cannot be extracted from stretched exponential kinetics observed in the ensemble.

In this last section, we demonstrate that ABEL-2DFLCS is able to detect molecule-to-molecule lifetime heterogeneity within the DNA hairpin loop while also compensating for this heterogeneity through its robust analytical process. If heterogeneity exists within a population for a given parameter (in this case, the fluorescence lifetime), one would expect that an ensemble analysis, which incorrectly averaged this heterogeneous lifetime, would result in an artificial correlation of the lifetime with other measurements that are

dependent on the lifetime (Figure 5a,c). This scenario occurs because the true values of each molecule's different fluorescence lifetime are reduced to an ensemble-average: introducing a systemic error in further downstream analysis.

To clearly show this problem and solution, we simulated a data set where each molecule had a different closed-state lifetime. We then analyzed this data set of simulated single molecules via ensemble analysis (ensemble-based ABEL-2DFLCS, Figure 5a,b), where the photon streams for the entire data set were summed into a single 2DFLCS correlation map (analogous to Figure 1f) in order to obtain the lifetime distribution for the data set. This lifetime distribution obtained through ensemble-averaging was then used to obtain kinetic parameters for each event, an analysis procedure that is similar to ordinary 2DFLCS methods,^{26,27} and an analogous step is present in the procedure for high-resolution hidden Markov analysis.^{23–25} However, we observed that averaging the lifetime distributions for a data set with molecule-to-molecule diversity in lifetime, an experimentally relevant scenario (see below) resulted in a spurious correlation between the closed-state lifetime (Figure 5a, x-axis) and the equilibrium constant derived for each molecule (Figure 5a, y-axis). To remedy this issue, the simulated data set was then analyzed by creating a 2DFLCS correlation map for each individual molecule. Such a MBM analysis was made possible due to the long observation

time from the ABEL trap, and this analysis removed the correlation erroneously imposed by ensemble-averaging (Figure 5c). The Pearson coefficient (R) and the p -value of the null hypothesis (P) are shown in Figure 5 insets, which quantify the correlation between these parameters, and a simple linear fit is added to help visualize the removal of the correlation when transitioning from ensemble to MBM analysis. Importantly, the magnitude of P represents the probability of no correlation, and the value of R represents the strength of the correlation: the slope of the red line helps visualize whether a correlation exists but does not indicate the strength of the correlation. Lastly, the transition from ensemble-based measurements to a true MBM analysis of our simulated data set also improved how accurately the median value mapped to the true value of K_{eq} (Section SI.12). While the ensemble-based measurement (Figure 5a) incorrectly averages heterogeneous fluorescence lifetimes, it is important to note that, for a data set with hundreds of molecules, the MBM analysis is working with 100-fold fewer photons, and thus the distribution of those independent measurements is expected to be larger due to the reduction in signal (Figure 5c).

After using a simulated data set to show that ensemble-averaging a heterogeneous closed-state lifetime produces an erroneous correlation and that ABEL-2DFLCS's MBM analysis rectifies this artifactual correlation, the same two analytical methods (ensemble-based and MBM ABEL-2DFLCS) were repeated on the experimental data set of the T21 DNA hairpin (Figure 5b,d). Comparing the Pearson coefficient for the two methods shows that the correlation between equilibrium constant and lifetime remains (the null hypothesis, P , stays close to 0) but becomes substantially weakened upon transitioning from ensemble-averaged lifetime analysis to MBM analysis (the magnitude of the Pearson coefficient, R , is significantly reduced from 0.891 to 0.351). It should be noted that, while the correlation is reduced, it is not removed entirely from the system as in the case of the simulated data set (Figure 5a,c). This residual correlation likely occurs because, while the simulated data set was specifically designed to have no intrinsic correlation between parameters, no such guarantee can be made about the experimental T21 DNA hairpin system. Rather, the significantly different slopes between Figure 5b and d indicates the existence of heterogeneity in lifetime (closed and/or opened) and shows the use of ABEL-2DFLCS to independently analyze each molecule reduces those artifacts. Ensemble-based ABEL-2DFLCS analysis was also performed on a simulated data set that had no heterogeneity within its closed-state lifetimes (Section SI.13). This negative control shows that the correlation seen in Figure 5a is indeed a consequence of the lifetime heterogeneity within the data set, and not an artifact of the analysis. In summary, the MBM analysis of the T21 DNA hairpin (Figure 5d) reveals heterogeneity within the T21 hairpins' fluorescence lifetimes. That Figure 5d also shows a residual correlation between single-exponential fluorescence lifetime and equilibrium constant further suggests that this heterogeneity in fluorescence lifetime may also be correlated with the T21 DNA hairpin kinetics, possibly due to heterogeneity in the K_{eq} among the T21 DNA hairpin that was not present in the simulated data set. This correlation makes sense, as a larger equilibrium constant K_{eq} would suggest more time spent in the closed configuration, and thus more time in a quenched FRET state and a lower observed fluorescence lifetime.

Finally, we performed ABEL-2DFLCS on a mixture of T21 and T8 hairpins to show that their populations could be resolved at the single-molecule level through measuring their kinetic properties. Briefly, the mixture data set was parsed into two areas that matched their expected fluorescence properties (see Section SI.16), and 10 events from each area (20 total) were selected. This allowed us to sort the T21/T8 mixture into populations based on fluorescence properties while remaining agnostic to their kinetic properties. ABEL-2DFLCS analysis was then used to derive the kinetic properties of these events as shown in Figure 6, with the T21 and T8 events shown in green

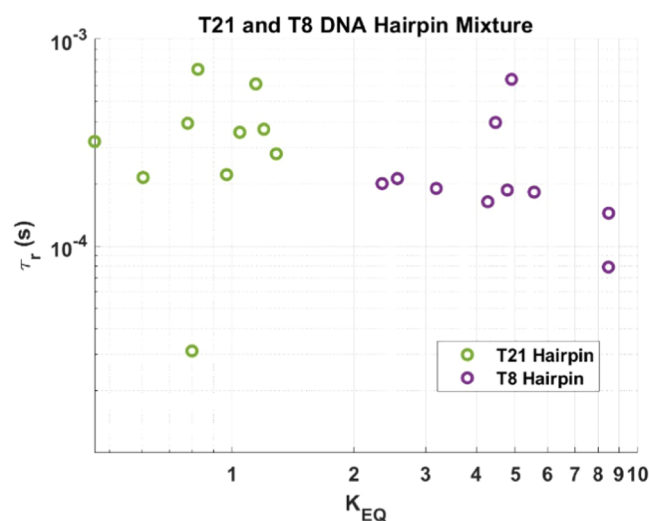


Figure 6. Reaction time constants and equilibrium constants of molecules assigned as T21 (green, $N = 10$) and T8 (purple, $N = 10$).

and purple, respectively. Despite the T8 hairpin loop having a large K_{eq} value (and thus being difficult to quantify the relative photon contribution from the sparsely populated opened state), it can be seen that the populations are clearly resolved from each other and have kinetic values comparable to those measured from the nonmixed samples.

CONCLUSIONS

In this work we used ABEL-2DFLCS to accurately characterize the structural dynamics of a FRET-labeled biomolecule, a DNA hairpin. We quantified submillisecond time scale dynamics on a molecule-by-molecule level without relying on ensemble-averaging data across multiple single-molecule measurements, a process that was also vetted on simulated data sets. To our knowledge, this is the first experiment that has achieved this milestone. For the specific hairpin studied, the kinetics revealed a simple two-state interconversion without significant static or dynamic kinetic heterogeneity, in contrast to some previous results, where the molecule-by-molecule analysis of ABEL-2DFLCS avoided artifacts caused by inhomogeneity in lifetime and spatial excitation. We further showed the ability of ABEL-2DFLCS to parse kinetics of inherently heterogeneous systems by resolving the kinetics from a mixture of T21 and T8 hairpins. More generally, this analysis can be performed on any solution-phase biomolecule with conformational states characterized by different lifetimes, a scenario easily achieved with the use of FRET labels, and can be applied to many highly fluctuating, biologically relevant systems such as intrinsically disordered proteins, molecule motors, and enzymes, fulfilling an outstanding need in the

community for true molecule-by-molecule elucidation of fast solution-phase dynamics.

■ ASSOCIATED CONTENT

Supporting Information

The Supporting Information is available free of charge at <https://pubs.acs.org/doi/10.1021/acspchemau.3c00066>.

Additional experimental details, information on DNA constructs, additional analysis details and error propagation, and additional simulations (PDF)

■ AUTHOR INFORMATION

Corresponding Author

Randall H. Goldsmith – Department of Chemistry, University of Wisconsin—Madison, Madison, Wisconsin 53706, United States; orcid.org/0000-0001-9083-8592; Email: rhg@chem.wisc.edu

Authors

Alexander K. Foote – Department of Chemistry, University of Wisconsin—Madison, Madison, Wisconsin 53706, United States

Kunihiko Ishii – Molecular Spectroscopy Laboratory, RIKEN, Wako, Saitama 351-0198, Japan; Ultrafast Spectroscopy Research Team, RIKEN Center for Advanced Photonics (RAP), Wako, Saitama 351-0198, Japan; orcid.org/0000-0001-5714-5997

Brendan Cullinane – Department of Chemistry, University of Wisconsin—Madison, Madison, Wisconsin 53706, United States

Tahei Tahara – Molecular Spectroscopy Laboratory, RIKEN, Wako, Saitama 351-0198, Japan; Ultrafast Spectroscopy Research Team, RIKEN Center for Advanced Photonics (RAP), Wako, Saitama 351-0198, Japan; orcid.org/0000-0002-6340-8535

Complete contact information is available at: <https://pubs.acs.org/10.1021/acspchemau.3c00066>

Author Contributions

^{||}A.K.F. and K.I. contributed equally to this work.

Notes

The authors declare no competing financial interest.

■ ACKNOWLEDGMENTS

This work was supported by the National Institute of Health (NIH) Grant Number R01GM136981, the JSPS KAKENHI Grant Number JP21H01897, and a grant of the Morino Foundation for Molecular Science (to K.I.).

■ REFERENCES

- (1) Neuweiler, H.; Schulz, A.; Böhmer, M.; Enderlein, J.; Sauer, M. Measurement of Submicrosecond Intramolecular Contact Formation in Peptides at the Single-Molecule Level. *J. Am. Chem. Soc.* **2003**, *125* (18), 5324–5330.
- (2) Michalet, X.; Weiss, S.; Jäger, M. Single-Molecule Fluorescence Studies of Protein Folding and Conformational Dynamics. *Chem. Rev.* **2006**, *106* (5), 1785–1813.
- (3) Guo, J.; Zhou, H. X. Protein Allostery and Conformational Dynamics. *Chem. Rev.* **2016**, *116* (11), 6503–6515.
- (4) Su, H.; Brockman, J. M.; Duan, Y.; Sen, N.; Chhabra, H.; Bazrafshan, A.; Blanchard, A. T.; Meyer, T.; Andrews, B.; Doye, J. P. K.; Ke, Y.; Dyer, R. B.; Salaita, K. Massively Parallelized Molecular Force Manipulation with On-Demand Thermal and Optical Control. *J. Am. Chem. Soc.* **2021**, *143* (46), 19466–19473.
- (5) Maria-Solano, M. A.; Serrano-Hervás, E.; Romero-Rivera, A.; Iglesias-Fernández, J.; Osuna, S. Role of Conformational Dynamics in the Evolution of Novel Enzyme Function. *Chem. Commun.* **2018**, *54* (50), 6622–6634.
- (6) Kovermann, M.; Rogne, P.; Wolf-Watz, M. Protein Dynamics and Function from Solution State NMR Spectroscopy. *Q. Rev. Biophys.* **2016**, *49*, No. e6.
- (7) Henzler-Wildman, K. A.; Lei, M.; Thai, V.; Kerns, S. J.; Karplus, M.; Kern, D. A Hierarchy of Timescales in Protein Dynamics Is Linked to Enzyme Catalysis. *Nature* **2007**, *450* (7171), 913–916.
- (8) Torchia, D. A. Protein Dynamics from NMR Relaxation. *eMagRes* **2007**, *2007* (9), 7–10.
- (9) Onuchic, J. N.; Luthey-Schulten, Z.; Wolynes, P. G. Theory of Protein Folding: The Energy Landscape Perspective. *Annu. Rev. Phys. Chem.* **1997**, *48* (1), 545–600.
- (10) Eaton, W. A. Modern Kinetics and Mechanism of Protein Folding: A Retrospective. *J. Phys. Chem. B* **2021**, *125* (14), 3452–3467.
- (11) Brucala, M.; Schuler, B.; Samorì, B. Single-Molecule Studies of Intrinsically Disordered Proteins. *Chem. Rev.* **2014**, *114* (6), 3281–3317.
- (12) Mazal, H.; Haran, G. Single-Molecule FRET Methods to Study the Dynamics of Proteins at Work. *Curr. Opin. Biomed. Eng.* **2019**, *12*, 8–17.
- (13) Lerner, E.; Cordes, T.; Ingargiola, A.; Alhadid, Y.; Chung, S. Y.; Michalet, X.; Weiss, S. Toward Dynamic Structural Biology: Two Decades of Single-Molecule Förster Resonance Energy Transfer. *Science* **2018**, *359* (6373), No. eaan1133, DOI: [10.1126/science.aan1133](https://doi.org/10.1126/science.aan1133).
- (14) Ha, T.; Enderle, T.; Ogletree, D. F.; Chemla, D. S.; Selvin, P. R.; Weiss, S. Probing the Interaction between Two Single Molecules: Fluorescence Resonance Energy Transfer between a Single Donor and a Single Acceptor. *Proc. Natl. Acad. Sci. U.S.A.* **1996**, *93* (13), 6264–6268.
- (15) Basu, A.; Bobrovnikov, D. G.; Qureshi, Z.; Kayikcioglu, T.; Ngo, T. T. M.; Ranjan, A.; Eustermann, S.; Cieza, B.; Morgan, M. T.; Hejna, M.; Rube, H. T.; Hopfner, K. P.; Wolberger, C.; Song, J. S.; Ha, T. Measuring DNA Mechanics on the Genome Scale. *Nature* **2021**, *589* (7842), 462–467.
- (16) Schwille, P. Fluorescence Correlation Spectroscopy and Its Potential for Intracellular Applications. *Cell Biochem. Biophys.* **2001**, *34* (3), 383–408.
- (17) Jazani, S.; Sgouralis, I.; Shafraz, O. M.; Levitus, M.; Sivasankar, S.; Pressé, S. An Alternative Framework for Fluorescence Correlation Spectroscopy. *Nat. Commun.* **2019**, *10* (1), No. 3662.
- (18) Xu, L. W. Q.; Jazani, S.; Kilic, Z.; Pressé, S. *Single-Molecule Reaction-Diffusion*; bioRxiv, 2023. DOI: [10.1101/2023.09.05.556378](https://doi.org/10.1101/2023.09.05.556378) (accessed May 01, 2023).
- (19) Chung, H. S.; McHale, K.; Louis, J. M.; Eaton, W. A. Single-Molecule Fluorescence Experiments Determine Protein Folding Transition Path Times. *Science* **2012**, *335* (6071), 981–984.
- (20) Kondo, T.; Gordon, J. B.; Pinnola, A.; Dall’Osto, L.; Bassi, R.; Schlau-Cohen, G. S. Microsecond and Millisecond Dynamics in the Photosynthetic Protein LHCSR1 Observed by Single-Molecule Correlation Spectroscopy. *Proc. Natl. Acad. Sci. U.S.A.* **2019**, *116* (23), 11247–11252.
- (21) Hoffmann, A.; Nettels, D.; Clark, J.; Borgia, A.; Radford, S. E.; Clarke, J.; Schuler, B. Quantifying Heterogeneity and Conformational Dynamics from Single Molecule FRET of Diffusing Molecules: Recurrence Analysis of Single Particles (RASP). *Phys. Chem. Chem. Phys.* **2011**, *13* (5), 1857–1871.
- (22) Oikawa, H.; Suzuki, Y.; Saito, M.; Kamagata, K.; Arai, M.; Takahashi, S. Microsecond Dynamics of an Unfolded Protein by a Line Confocal Tracking of Single Molecule Fluorescence. *Sci. Rep.* **2013**, *3*, No. 2151.

- (23) Pirchi, M.; Tsukanov, R.; Khamis, R.; Tomov, T. E.; Berger, Y.; Khara, D. C.; Volkov, H.; Haran, G.; Nir, E. Photon-by-Photon Hidden Markov Model Analysis for Microsecond Single-Molecule FRET Kinetics. *J. Phys. Chem. B* **2016**, *120* (51), 13065–13075.
- (24) Aviram, H. Y.; Pirchi, M.; Mazal, H.; Barak, Y.; Riven, I.; Haran, G. Direct Observation of Ultrafast Large-Scale Dynamics of an Enzyme under Turnover Conditions. *Proc. Natl. Acad. Sci. U.S.A.* **2018**, *115* (13), 3243–3248.
- (25) Mazal, H.; Iljina, M.; Barak, Y.; Elad, N.; Rosenzweig, R.; Goloubinoff, P.; Riven, I.; Haran, G. Tunable Microsecond Dynamics of an Allosteric Switch Regulate the Activity of a AAA+ Disaggregation Machine. *Nat. Commun.* **2019**, *10* (1), No. 2151, DOI: 10.1038/s41467-019-09474-6.
- (26) Ishii, K.; Tahara, T. Two-Dimensional Fluorescence Lifetime Correlation Spectroscopy. 1. Principle. *J. Phys. Chem. B* **2013**, *117* (39), 11414–11422.
- (27) Ishii, K.; Tahara, T. Two-Dimensional Fluorescence Lifetime Correlation Spectroscopy. 2. Application. *J. Phys. Chem. B* **2013**, *117* (39), 11423–11432.
- (28) Troiano, J. M.; Perozeni, F.; Moya, R.; Zuliani, L.; Baek, K.; Jin, E.; Cazzaniga, S.; Ballottari, M.; Schlau-Cohen, G. S. Identification of 1 Distinct PH- and Zeaxanthin-Dependent Quenching in LHCSR3 from *Chlamydomonas Reinhardtii*. *eLife* **2021**, *10*, 1–59.
- (29) Otsu, T.; Ishii, K.; Oikawa, H.; Arai, M.; Takahashi, S.; Tahara, T. Highly Heterogeneous Nature of the Native and Unfolded States of the B Domain of Protein A Revealed by Two-Dimensional Fluorescence Lifetime Correlation Spectroscopy. *J. Phys. Chem. B* **2017**, *121* (22), 5463–5473.
- (30) Otsu, T.; Ishii, K.; Tahara, T. Microsecond Protein Dynamics Observed at the Single-Molecule Level. *Nat. Commun.* **2015**, *6*, No. 7685.
- (31) Sarkar, B.; Ishii, K.; Tahara, T. Microsecond Conformational Dynamics of Biopolymers Revealed by Dynamic-Quenching Two-Dimensional Fluorescence Lifetime Correlation Spectroscopy with Single Dye Labeling. *J. Phys. Chem. Lett.* **2019**, *10* (18), 5536–5541.
- (32) Cheng, C. H.; Ishii, K.; Tahara, T. Microsecond Equilibrium Dynamics of Hairpin-Forming Oligonucleotides Quantified by Two-Color Two-Dimensional Fluorescence Lifetime Correlation Spectroscopy. *J. Phys. Chem. B* **2020**, *124* (47), 10673–10681.
- (33) Cohen, A. E.; Moerner, W. E. Method for Trapping and Manipulating Nanoscale Objects in Solution. *Appl. Phys. Lett.* **2005**, *86* (9), No. 093109, DOI: 10.1063/1.1872220.
- (34) Cohen, A. E.; Moerner, W. E. Controlling Brownian Motion of Single Protein Molecules and Single Fluorophores in Aqueous Buffer. *Opt. Express* **2008**, *16* (10), 6941–6956.
- (35) Wang, Q.; Goldsmith, R. H.; Jiang, Y.; Bockenhauer, S. D.; Moerner, W. E. Probing Single Biomolecules in Solution Using the Anti-Brownian Electrokinetic (ABEL) Trap. *Acc. Chem. Res.* **2012**, *45* (11), 1955–1964.
- (36) Peng, S.; Wang, W.; Chen, C. Surface Transient Binding-Based Fluorescence Correlation Spectroscopy (STB-FCS), a Simple and Easy-to-Implement Method to Extend the Upper Limit of the Time Window to Seconds. *J. Phys. Chem. B* **2018**, *122* (18), 4844–4850.
- (37) Yin, Y.; Wang, P.; Yang, X. X.; Li, X.; He, C.; Zhao, X. S. Panorama of DNA Hairpin Folding Observed via Diffusion-Decelerated Fluorescence Correlation Spectroscopy. *Chem. Commun.* **2012**, *48* (59), 7413–7415.
- (38) Talaga, D. S.; Lau, W. L.; Roder, H.; Tang, J.; Jia, Y.; DeGrado, W. F.; Hochstrasser, R. M. Dynamics and Folding of Single Two-Stranded Coiled-Coil Peptides Studied by Fluorescent Energy Transfer Confocal Microscopy. *Proc. Natl. Acad. Sci. U.S.A.* **2000**, *97* (24), 13021–13026.
- (39) Rasnik, I.; McKinney, S. A.; Ha, T. Surfaces and Orientations: Much to FRET About? *Acc. Chem. Res.* **2005**, *38* (7), 542–548.
- (40) Friedel, M.; Baumketner, A.; Shea, J.-E. Effects of Surface Tethering on Protein Folding Mechanisms. *Proc. Natl. Acad. Sci. U.S.A.* **2006**, *103* (22), 8396–8401.
- (41) Goldsmith, R. H.; Moerner, W. E. Watching Conformational- and Photo-Dynamics of Single Fluorescent Proteins in Solution. *Nat. Chem.* **2010**, *2* (3), 179–186.
- (42) Manger, L. H.; Foote, A. K.; Wood, S. L.; Holden, M. R.; Heylman, K. D.; Margittai, M.; Goldsmith, R. H. Revealing Conformational Variants of Solution-Phase Intrinsically Disordered Tau Protein at the Single-Molecule Level. *Angew. Chem., Int. Ed.* **2017**, *56* (49), 15584–15588.
- (43) Foote, A. K.; Manger, L. H.; Holden, M. R.; Margittai, M.; Goldsmith, R. H. Time-Resolved Multirotational Dynamics of Single Solution-Phase Tau Proteins Reveals Details of Conformational Variation. *Phys. Chem. Chem. Phys.* **2019**, *21* (4), 1863–1871.
- (44) Wilson, H.; Wang, Q. ABEL-FRET: Tether-Free Single-Molecule FRET with Hydrodynamic Profiling. *Nat. Methods* **2021**, *18* (7), 816–820.
- (45) Schlau-Cohen, G. S.; Wang, Q.; Southall, J.; Cogdell, R. J.; Moerner, W. E. Single-Molecule Spectroscopy Reveals Photosynthetic LH2 Complexes Switch between Emissive States. *Proc. Natl. Acad. Sci. U.S.A.* **2013**, *110* (27), 10899–10903.
- (46) Squires, A. H.; Dahlberg, P. D.; Liu, H.; Magdaong, N. C. M.; Blankenship, R. E.; Moerner, W. E. Single-Molecule Trapping and Spectroscopy Reveals Photophysical Heterogeneity of Phycobilisomes Quenched by Orange Carotenoid Protein. *Nat. Commun.* **2019**, *10* (1), No. 1172, DOI: 10.1038/s41467-019-09084-2.
- (47) Heitkamp, T.; Börsch, M. Fast ATP-Dependent Subunit Rotation in Reconstituted FoF1-ATP Synthase Trapped in Solution. *J. Phys. Chem. B* **2021**, *125* (28), 7638–7650.
- (48) Dienerowitz, M.; Howard, J. A. L.; Quinn, S. D.; Dienerowitz, F.; Leake, M. C. Single-Molecule FRET Dynamics of Molecular Motors in an ABEL Trap. *Methods* **2021**, *193*, 96–106.
- (49) Chu, J.; Ejaz, A.; Lin, K. M.; Joseph, M. R.; Coraor, A. E.; Drummond, D. A.; Squires, A. H. Single-Molecule Fluorescence Multiplexing by Multi-Parameter Spectroscopic Detection of Nanostructured FRET Labels. 2024, arXiv:2307.01614. arXiv.org e-Print archive. <https://arxiv.org/abs/2307.01614> (accessed May 01, 2023).
- (50) Wang, Q.; Moerner, W. E. An Adaptive Anti-Brownian Electrokinetic Trap with Real-Time Information on Single-Molecule Diffusivity and Mobility. *ACS Nano* **2011**, *5* (7), 5792–5799.
- (51) Wang, Q.; Moerner, W. E. Single-Molecule Motions Enable Direct Visualization of Biomolecular Interactions in Solution. *Nat. Methods* **2014**, *11* (5), 555–558.
- (52) Squires, A. H.; Lavania, A. A.; Dahlberg, P. D.; Moerner, W. E. Interferometric Scattering Enables Fluorescence-Free Electrokinetic Trapping of Single Nanoparticles in Free Solution. *Nano Lett.* **2019**, *19* (6), 4112–4117.
- (53) Otsu, T.; Yamaguchi, S. Two-Dimensional Fluorescence Lifetime Correlation Spectroscopy: Concepts and Applications. *Molecules* **2018**, *23* (11), No. 2972, DOI: 10.3390/molecules23112972.
- (54) Watkins, L. P.; Yang, H. Detection of Intensity Change Points in Time-Resolved Single-Molecule Measurements. *J. Phys. Chem. B* **2005**, *109* (1), 617–628.
- (55) Livesey, A. K.; Brochon, J. C. Analyzing the Distribution of Decay Constants in Pulse-Fluorimetry Using the Maximum Entropy Method. *Biophys. J.* **1987**, *52* (5), 693–706.
- (56) Brochon, J. C. Maximum Entropy Method of Data Analysis in Time-Resolved Spectroscopy. *Part B: Numerical Computer Methods, Methods in Enzymology*; Elsevier, 1994; Vol. 240, pp 262–311.
- (57) Böhmer, M.; Wahl, M.; Rahn, H.-J.; Erdmann, R.; Enderlein, J. Time-Resolved Fluorescence Correlation Spectroscopy. *Chem. Phys. Lett.* **2002**, *353* (5–6), 439–445.
- (58) Gregor, I.; Enderlein, J. Time-Resolved Methods in Biophysics. 3. Fluorescence Lifetime Correlation Spectroscopy. *Photochem. Photobiol. Sci.* **2007**, *6* (1), 13–18.
- (59) Felekyan, S.; Kalinin, S.; Sanabria, H.; Valeri, A.; Seidel, C. A. M. Filtered FCS: Species Auto- and Cross-Correlation Functions Highlight Binding and Dynamics in Biomolecules. *ChemPhysChem* **2012**, *13* (4), 1036–1053.

- (60) Harvey, B. J.; Perez, C.; Levitus, M. DNA Sequence-Dependent Enhancement of Cy3 Fluorescence. *Photochem. Photobiol. Sci.* **2009**, *8* (8), 1105–1110.
- (61) Widengren, J.; Schwille, P. Characterization of Photoinduced Isomerization and Back-Isomerization of the Cyanine Dye Cy5 by Fluorescence Correlation Spectroscopy. *J. Phys. Chem. A* **2000**, *104* (27), 6416–6428.
- (62) Bonnet, G.; Krichevsky, O.; Libchaber, A. Kinetics of Conformational Fluctuations in DNA Hairpin-Loops. *Proc. Natl. Acad. Sci. U.S.A.* **1998**, *95* (15), 8602–8606.
- (63) Goddard, N. L.; Bonnet, G.; Krichevsky, O.; Libchaber, A. Sequence Dependent Rigidity of Single Stranded DNA. *Phys. Rev. Lett.* **2000**, *85* (11), 2400–2403.
- (64) Jung, J.; Van Orden, A. Folding and Unfolding Kinetics of DNA Hairpins in Flowing Solution by Multiparameter Fluorescence Correlation Spectroscopy. *J. Phys. Chem. B* **2005**, *109* (8), 3648–3657.
- (65) Jung, J.; Van Orden, A. A Three-State Mechanism for DNA Hairpin Folding Characterized by Multiparameter Fluorescence Fluctuation Spectroscopy. *J. Am. Chem. Soc.* **2006**, *128* (4), 1240–1249.
- (66) Melnykov, A. V.; Nayak, R. K.; Hall, K. B.; Van Orden, A. Effect of Loop Composition on the Stability and Folding Kinetics of RNA Hairpins with Large Loops. *Biochemistry* **2015**, *54* (10), 1886–1896.
- (67) Abdollah-Nia, F.; Gelfand, M. P.; Van Orden, A. Three-State Dna Hairpin Conformational Dynamics Revealed by Higher-Order Fluorescence Correlation Spectroscopy. *J. Phys. Chem. B* **2019**, *123* (7), 1491–1504.
- (68) Nayak, R. K.; Peersen, O. B.; Hall, K. B.; Van Orden, A. Millisecond Time-Scale Folding and Unfolding of DNA Hairpins Using Rapid-Mixing Stopped-Flow Kinetics. *J. Am. Chem. Soc.* **2012**, *134* (5), 2453–2456.
- (69) Torres, T.; Levitus, M. Measuring Conformational Dynamics: A New FCS-FRET Approach. *J. Phys. Chem. B* **2007**, *111* (25), 7392–7400.
- (70) Wallace, M. I.; Ying, L.; Balasubramanian, S.; Klenerman, D. FRET Fluctuation Spectroscopy: Exploring the Conformational Dynamics of a DNA Hairpin Loop. *J. Phys. Chem. B* **2000**, *104* (48), 11551–11555.
- (71) Gurnathan, K.; Levitus, M. Chapter 2 Applications of Fluorescence Correlation Spectroscopy to the Study of Nucleic Acid Conformational Dynamics. *Progress in Nucleic Acid Research and Molecular Biology*; Elsevier, 2008; Vol. 82.
- (72) Wallace, M. I.; Ying, L.; Balasubramanian, S.; Klenerman, D. Non-Arrhenius Kinetics for the Loop Closure of a DNA Hairpin. *Proc. Natl. Acad. Sci. U.S.A.* **2001**, *98* (10), 5584–5589.
- (73) Ying, L.; Wallace, M. I.; Klenerman, D. Two-State Model of Conformational Fluctuation in a DNA Hairpin-Loop. *Chem. Phys. Lett.* **2001**, *334* (1–3), 145–150.
- (74) Gurnathan, K.; Levitus, M. FRET Fluctuation Spectroscopy of Diffusing Biopolymers: Contributions of Conformational Dynamics and Translational Diffusion. *J. Phys. Chem. B* **2010**, *114* (2), 980–986.
- (75) Kügel, W.; Muschielok, A.; Michaelis, J. Bayesian-Inference-Based Fluorescence Correlation Spectroscopy and Single-Molecule Burst Analysis Reveal the Influence of Dye Selection on DNA Hairpin Dynamics. *ChemPhysChem* **2012**, *13* (4), 1013–1022.